American Journal of
Biomedical Science & Research

www.biomedgrid.com
ISSN: 2642-1747

Research Article

Identification and Characterization of Ribosomal Stress Related Signature Genes in Ovarian Cancer Using Bioinformatics Analysis and Machine Learning

Xuechuan Han, Yan Yu, Yang Fan*

Department of Obstetrics and Gynecology, People's Hospital of Ningxia Hui Autonomous Region, Ningxia Medical University, China

***Corresponding author:** Yang Fan, Department of Obstetrics and Gynecology, People's Hospital of Ningxia Hui Autonomous Region, Zhengyuan North Street, Jinfeng District, Yinchuan City, Ningxia Hui Autonomous Region, China.

To Cite This article: *Xuechuan Han, Yan Yu, Yang Fan*, Identification and Characterization of Ribosomal Stress Related Signature Genes in Ovarian Cancer Using Bioinformatics Analysis and Machine Learning. Am J Biomed Sci & Res. 2026 31(4) AJBSR.MS.ID.004066,*

DOI: 10.34297/AJBSR.2026.31.004066

Received: June 29, 2026 **Published:** July 06, 2026

Abstract

Introduction: Ovarian Cancer (OC) is a highly aggressive malignancy with poor prognosis. Ribosomal stress, a cellular response to disrupted ribosome biogenesis, has been increasingly implicated in tumorigenesis. Yet its contribution to OC remains unclear.

Method and Material: We integrated four GEO transcriptomic datasets and identified Ribosomal Stress Related Signature Genes (RSRGs) through differential expression. To construct a robust diagnostic model, three machine learning algorithms: LASSO regression, Support Vector Machine Recursive Feature Elimination (SVM-RFE), and random forest were combined.

Result: A total of 117 differentially expressed RSRGs were identified, mainly enriched in cytoskeletal regulation, lipid metabolism, proteoglycan signaling, and IL-17 mediated inflammatory pathways. The integrated machine learning approach identified six feature genes (SPP1, MAPK13, LCN2, JUP, DSP, and BMP6). Immune profiling revealed increased macrophage M0/M2 and decreased CD8+ T cell infiltration in high-risk samples, with SPP1, MAPK13, and DSP positively correlated with macrophage abundance.

Conclusion: This study identifies a six-gene ribosomal stress signature linking tumor intrinsic pathways and immune remodeling in OC. Especially SPP1 is the potential of targeting ribosomal stress and a therapeutic strategy in ovarian cancer.

Keywords: Ovarian cancer, Ribosomal stress, Machine learning, Bioinformatics Analysism, SPP1

Introduction

Ovarian cancer is an aggressive disease that is frequently detected at advanced stages. Globally, the incidence of OC, which includes cancers arising from the ovary, the fallopian tube and the peritoneum, is 313,959 instances per year, with 207,252 deaths per year1.It is initially very responsive to platinum-based chemotherapy [1-4]. However, the majority of patients relapse following initial surgery and chemotherapy, highlighting the urgent need to develop new therapeutic strategies. Nevertheless, the realization that ovarian cancer is composed of several different subtypes with different molecular landscapes [5,6], improved understanding of the genomics of these subtypes, and the development of new active biologic agents all have the promise of improving ovarian cancer outcomes and mortality.

Ribosome biogenesis is a multistep process that starts in the nucleolus and culminates in the formation of functional ribosomes in the cell. Ribosomes serve as translation machinery in the cell and

are a complex assembly of rRNAs and a large number of ribosomal proteins and ribosome-associated proteins. In humans, ribosomes comprise a small 40S subunit and a large 60S subunit. Evidence has emerged in recent decades regarding the close link between dysregulated ribosome biogenesis and tumorigenesis [7].For example, oncogenic c-Myc transcription factor increases protein synthesis and promotes translational capacity by modulating the expression of many genes implicated in ribosome biogenesis .Conversely, surveillance systems centered on tumor suppressors (e.g., TP53, PTEN, and RB1) have evolved in normal cells to oppose excessive changes in ribosome biosynthesis and halt cell growth. Aberrations in ribosomal proteins are documented in multiple ribosomopathies and cancer. This is suggestive of a potential for monitoring ribosomal proteins in prognosticating chemo/radio resistance of tumor cells. Therefore, it would investigate the utility of genetic screening of ribosoalproteins in treatment-native patients with cancer.

However, their role in ovarian cancer remains largely unexplored. Concurrently, Machine Learning (ML) has revolutionized cancer genomics by enabling high-dimensional data integration and the discovery of key diagnostic and prognostic biomarkers [8]. Integrating ML with ribosomal stress related gene profiling may therefore uncover novel OC-associated molecular features and provide new insights into tumor biology. Given these considerations, this study aims to identify ribosomal stress related signature genes in ovarian cancer using a multi-machine learning approach and to comprehensively characterize their association with OC. Our findings are expected to provide new insights into the molecular basis of ovarian cancer and contribute to the development of more effective diagnostic and therapeutic strategies

Materials and Methods

Data Sources and Preprocessing of Expression Profiles

Four ovarian cancer-related gene expression datasets (GSE6008, GSE4122, GSE12470, and GSE66957) were downloaded from the public Gene Expression Omnibus (GEO) database. These datasets included OC tissues and normal control samples obtained from different experimental platforms, aiming to improve the stability and generalizability of the results through integrated multi-dataset analysis. All raw expression matrix files were combined with corresponding clinical information files for sample classification and annotation (see Supplementary File S1). To ensure cross-platform comparability, the raw expression matrices of each dataset were preprocessed. The avereps () function in the limma package was used to merge and average duplicate probe signals. The necessity of log2 transformation was then determined: if the interquartile range exceeded a predefined threshold or if the 99th percentile was greater than 100, the data were considered untransformed, and a log2(x+1) conversion was automatically applied. Background correction and intensity normalization were then performed using the normalize Between Arrays () function to eliminate technical bias. The resulting normalized gene expression profiles were used for subsequent integrated analyses.

Batch Effect Correction and Principal Component Analysis (PCA)

This study used the ComBat algorithm (based on the sva package) to perform batch effect correction. The specific procedure included the following steps: extracting the common genes from the four datasets as the intersection gene set, constructing an initial merged matrix containing all samples, and then using the ComBat () function to estimate and adjust parameters under known batch labels to generate the batch-corrected expression matrix. This process effectively improved the comparability of data from different sources. To further verify the effect of batch correction, Principal Component Analysis (PCA) was used to visualize the distribution pattern of samples in high-dimensional space. A customized function, bioPCA (), was applied to draw PCA plots before and after batch correction ("Before batch correction" and "After batch correction"). This function performed dimensionality reduction using the prcomp () function and plotted scatter diagrams with the ggplot2 and ggpubr packages, with colors and shapes representing different dataset sources. Ideally, after correction, samples should cluster according to biological status rather than dataset origin, indicating successful removal of batch interference.

Differential Expression Analysis

Based on the batch-corrected integrated expression matrix, differential expression analysis was performed. Sample names were parsed to identify the corresponding project, sample ID, and group type. A design matrix was constructed, and linear model fitting was conducted using the lmFit function. The contrast condition "Treatment vs Control" was defined with make Contrasts, and empirical Bayes moderation (eBayes) was applied to calculate the t-statistics and adjusted p-values (FDR). The screening criteria were set as $|\log_2 \text{FoldChange}| > 1$ and adj.P.Value < 0.05, indicating at least a twofold change in expression with statistical significance after multiple testing correction. The resulting significant differentially expressed gene list and corresponding expression subset were generated for subsequent analyses.

Intersection Analysis of Differentially Expressed Genes and Ribosomal Stress Related Genes

Given that this study focused on the role of ribosomal stress in ovarian cancer, a set of reported Ribosomal Stress-Related Genes (RSRGs) was obtained from the GeneCards database (https://www.genecards.org/). The previously identified significantly Differentially Expressed Genes (DEGs) were intersected with this RSRG set to identify candidate genes that met both criteria-differential expression and involvement in ribosomal stress. These overlapping genes were defined as Differentially Expressed Ribosomal Stress-Related Genes (DE-RSRGs). The Venn Diagram package was used to generate a Venn diagram to visually illustrate the overlap between the two gene sets. The intersecting gene list was then exported and used as the primary input features for

subsequent machine learning modeling.

Functional Enrichment Analysis of DE-RSRGs

To elucidate the potential biological functions and pathway involvement of DE-RSRGs, Gene Ontology (GO) and Kyoto Encyclopedia of Genes and Genomes (KEGG) pathway enrichment analyses were performed. The intersecting gene symbols were first converted into Entrez IDs using the org.Hs.eg.db database. Subsequently, the enrichGO () and enrichKEGG () functions were applied to conduct hypergeometric tests. Terms with a q-value < 0.05 were considered significantly enriched. The enrichment results were visualized using bubble plots and customized circular plots, covering the three main GO categories: Biological Process (BP), Cellular Component (CC), and Molecular Function (MF), as well as key signaling pathways identified in the KEGG analysis.

Comparison of Three Machine Learning Models for Feature Gene Selection

To further narrow the range of candidate genes and enhance the predictive performance of diagnostic biomarkers, three mainstream machine learning algorithms were applied for feature selection:

Lasso Regression (Least Absolute Shrinkage and Selection Operator): This method is suitable for high-dimensional datasets with relatively small sample sizes. By applying L1 regularization, it shrinks the coefficients of less important variables to zero, achieving sparse modeling. The glmnet package was used to construct a binary logistic regression model, and the optimal λvalue was determined through cross-validation. Genes with nonzero coefficients were extracted as candidate features. Support Vector Machine-Recursive Feature Elimination (SVM-RFE): This approach combines the classification power of support vector machines with an iterative elimination strategy, sequentially removing the least important features to retain the most discriminative subset of genes. A custom R script (SHAP12.msvmRFE.R) was used to implement the algorithm, and the optimal number of features was determined based on the minimum cross-validation error criterion.

Random Forest (RF): As an ensemble learning method based on decision trees, random forest provides feature importance scores (Mean Decrease Accuracy or Gini Index). The random Forest package was used to train the classifier and generate a ranked list of gene importance, from which the top-ranked genes were selected as potential biomarkers. The intersection of these three gene sets was identified to determine the feature genes of ovarian cancer, defined as genes simultaneously selected by all three machine learning models. The VennDiagram package was used to visualize the overlap among the gene sets, and the intersecting genes were exported for subsequent consistency analysis and comprehensive evaluation. A box plot illustrated the differential expression of the feature genes between cancer (Treat) and normal (Control) groups, while a circos plot displayed the chromosomal locations of these feature genes.

Statistical Analysis

All analyses were performed in R (v4.4.1) and GraphPad Prism 7 (GraphPad Software, La Jolla, CA). Continuous variables were analyzed by t-test or Wilcoxon test as appropriate; categorical variables were analyzed by chi-square test. P < 0.05 was considered statistically significant.

Results

Data Preprocessing and Normalization Achieved High Quality

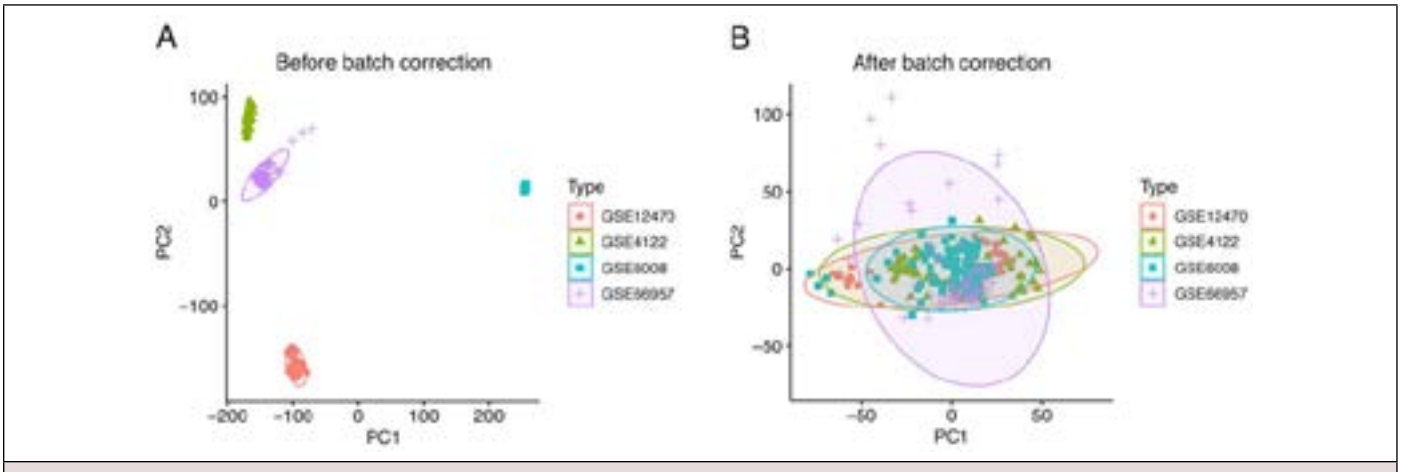

Note*: A: Before correction; B: After ComBat correction.

Figure 1: PCA Analysis Before and After Batch Effect Correction.

The raw expression matrices from the four GEO datasets were individually log-transformed and normalized the influence of extreme values and background noise was effectively eliminated. The results showed that after correction, the expression value distributions of all datasets became consistent, with smooth density curves concentrated within reasonable ranges, indicating high data quality suitable for subsequent integrative analysis. PCA revealed that, before correction, samples were clearly clustered according to their dataset origins, suggesting a strong batch effect (Figure 1A). After applying the ComBat algorithm, however, samples clustered mainly according to disease status (Control vs. Treat), and data from different sources were well integrated. This demonstrated effective batch effect correction, ensuring the reliability of the downstream differential expression analysis (Figure 1B).

Identification of DEGs

Differential expression analysis identified a total of 456 DEGs (adj.P.Value < 0.05, |logFC| > 1), including 267 upregulated and 189 downregulated genes (Figure 2A). A heatmap of the top 100 most significant DEGs (50 upregulated and 50 downregulated) further demonstrated strong sample discrimination, suggesting their potential biological relevance (Figure 2B).

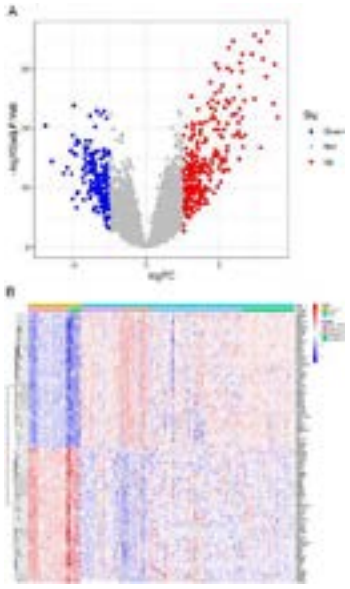

***Note:** A: Volcano plot;

B: Heatmap displaying expression patterns of the top 100 DEGs.

Figure 2: Differential Expression Analysis of Genes.

Identification of DE-RSRGs and Enriched in Key Functional Categories and Signaling Pathways

By intersecting the identified DEGs with RSRGs obtained from the GeneCards database, a total of 45 overlapping genes were identified, defined as DE-RSRGs. The Venn diagram clearly illustrated the overlap between the two gene sets. Although the intersecting region was relatively small, it was highly specific, indicating that these genes are not only aberrantly expressed in ovarian cancer but also directly involved in ribosomal function regulation (Figure 3A).

GO enrichment analysis revealed that DE-RSRGs were significantly associated with multiple core biological processes, including response to mechanical stimulus, regulation of cardiac muscle contraction, and cardiomyocyte action potential in BP; intercalated disc, cell-cell contact zone, and myofibril membrane in CC; as well as enzyme inhibitor activity, structural constituent of cytoskeleton, and integrin binding in MF (Figures 3B,3C). KEGG pathway analysis indicated that these genes were involved in classical pathways such as cytoskeleton organization in muscle cells, lipid metabolism and atherosclerosis, osteoclast differentiation, proteoglycans in cancer, and the IL-17 signaling pathway (Figure 3D).

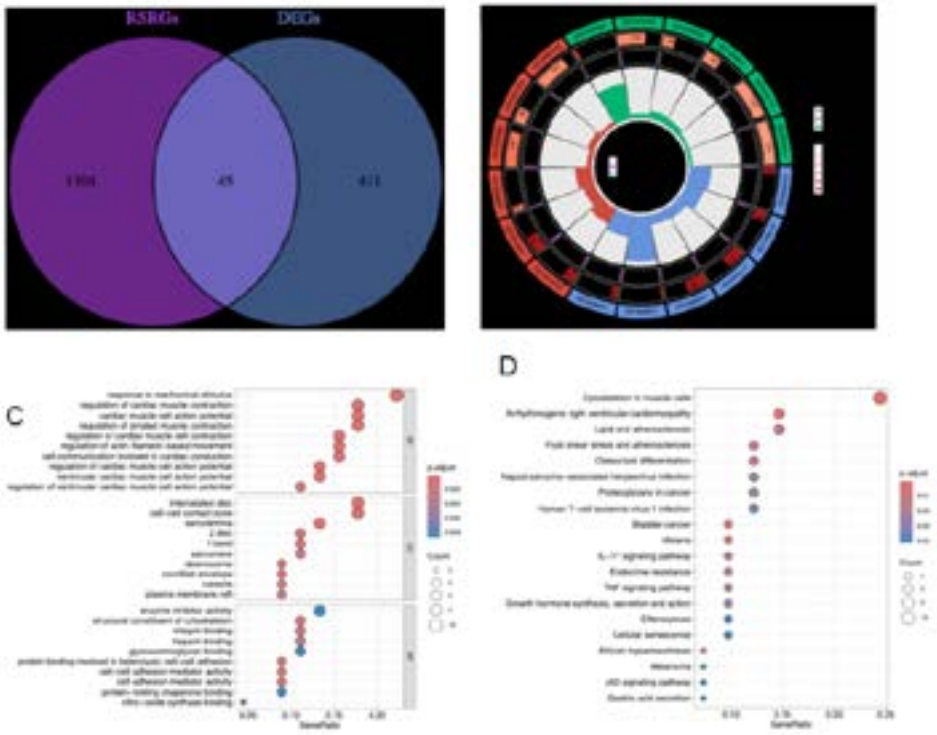

*Note: A: Venn diagram showing the intersection between DEGs and RSRGs;
B: circular plots;
C: Bubble plots of GO (BP/CC/MF) pathways enriched by DE-RSRGs (q < 0.05);
D: Bubble plots of KEGG pathways enriched by DE-RSRGs (q < 0.05).
Figure 3: Identification and Functional Enrichment of DE-RSRGs.

Machine Learning Models Identify a Robust Set of Feature Genes

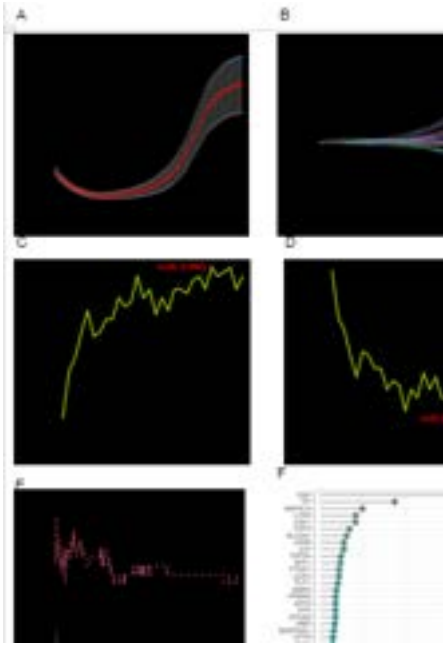

*Note: A, B: Lasso regression cross-validation error curve and coefficient shrinkage path;
C, D: SVM-RFE accuracy curve with varying feature numbers and the optimal gene subset;
E, F: Random Forest out-of-bag (OOB) error and gene importance ranking.
Figure 4: Feature Selection Using Machine Learning Models.

The three machine learning algorithms independently identified the most discriminative feature genes from the DE-RSRGs expression matrix: Lasso regression selected 18 genes, with the cross-validation error curve reaching its minimum at λ_min, indicating good model generalizability (Figures 4A, 4B). mSVM-RFE identified 25 key genes through recursive feature elimination. The cross-validation accuracy initially increased and then decreased as the number of features was reduced, with the peak indicating the optimal feature set (Figures 4C, 4D). Random forest ranked genes based on out-of-bag error, yielding the top 15 most important genes (Figures 4E, 4F).

By comparing the results of the three approaches, six ovarian cancer feature genes were ultimately defined: BMP6, DSP, JUP, LCN2, MAPK13, and SPP1 (Figure 5A). These genes were not only significantly differentially expressed but also consistently identified as core discriminative factors across multiple algorithms, highlighting their potential as novel biomarkers for ovarian cancer. A box plot illustrated the differential expression of these feature genes between cancer (Treat) and normal (Control) groups: DSP, JUP, LCN2, MAPK13, and SPP1 were upregulated in the Treat group, whereas BMP6 was downregulated compared to controls (Figure 5B). A circos plot displayed the chromosomal locations of the six feature genes (Figure 5C).

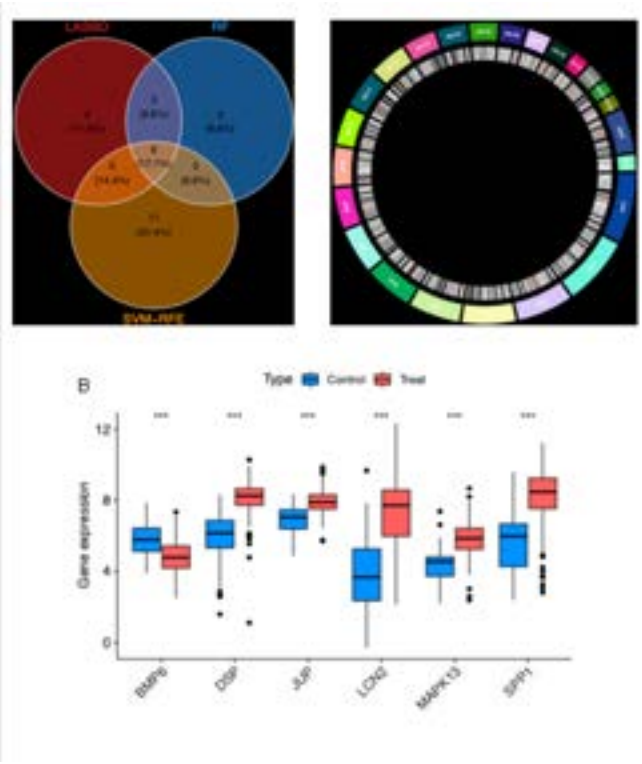

***Note:** A: Venn diagram showing the six feature genes shared by all three machine learning models;
B: Box plot illustrating differential expression of the feature genes between cancer and normal groups, ***p < 0.001;
C: Circos plot indicating the chromosomal locations of the feature genes.

Figure 5: Validation of Feature Genes.

Overall Immune Cell Infiltration Patterns and Group Differences in Ovarian Cancer Tissues

CIBERSORT analysis was performed on 172 ovarian cancer samples (including Control and Treat groups) to quantify the relative infiltration levels of 22 immune cell types in the tumor microenvironment. Stacked bar plots indicated that the major immune components included T cells (CD4+ memory T cells, regulatory T cells, γδ T cells), monocytes, macrophages (M0/M1/M2), Dendritic Cells (DCs), and Natural Killer (NK) cells. Considerable heterogeneity in immune composition was observed across samples, suggesting substantial inter-individual variability in immune responses (Figure 6A). Comparisons between the Control and Treat groups revealed statistically significant differences in multiple immune cell subsets (Figure 6B). Specifically, naive B cells, memory B cells, CD4 naive T cells, CD4 memory resting T cells, T follicular helper cells, monocytes, macrophages M0, macrophages M1, and resting mast cells differed significantly between groups (*p < 0.05, **p < 0.01, ***p < 0.001), with CD4 memory resting T cells and macrophages M1 showing the most pronounced differences. Other subsets, such as regulatory T cells, NK cells, and dendritic cells, showed no significant differences. These findings suggest that ovarian cancer may modulate specific immune cell subsets to influence anti-tumor immune responses.

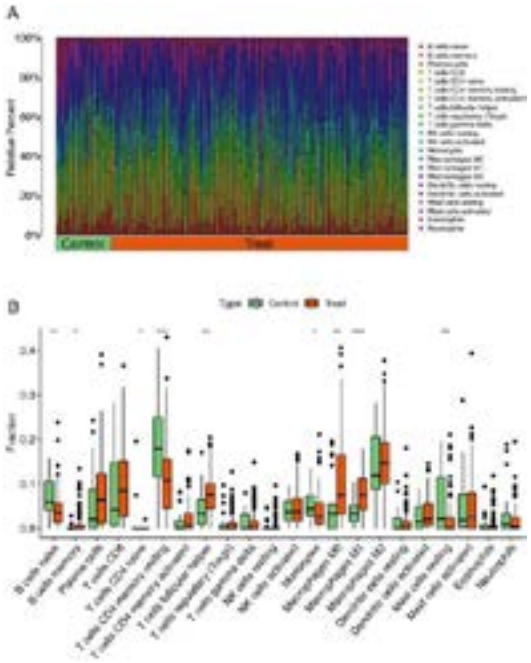

*Note: A: Stacked bar plot showing the distribution of 22 immune cell types across samples.

B: Box plot comparing immune cell subset differences between Control and Treat groups, *p < 0.05.

Figure 6: Immune Cell Infiltration Analysis.

Correlation Networks Among Immune Cells and Between Feature Genes and Immune Infiltrates in Ovarian Cancer

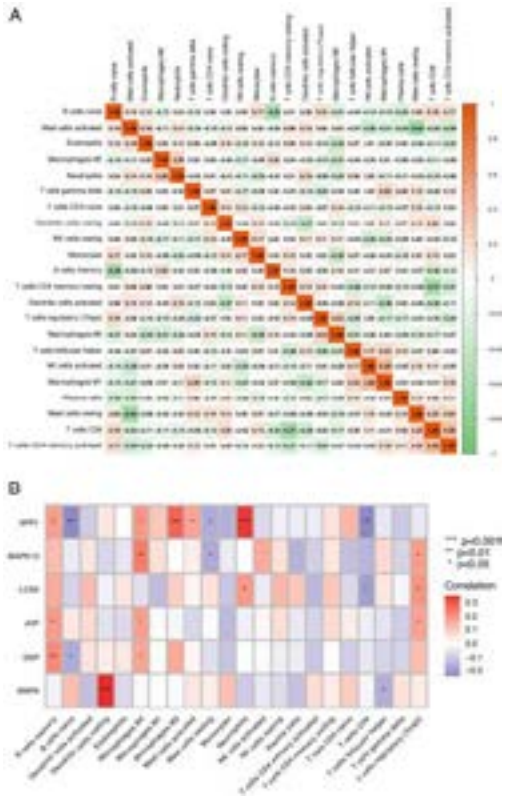

*Note: A: Spearman correlation heatmap among immune cell types, color gradient: red means positive, blue means negative; B: Correlation heatmap between feature genes and immune cell infiltration.

Figure 7: Correlation Networks.

Spearman correlation analysis was used to construct a correlation heatmap among immune cell types in the Treat group (Figure 7A). Results indicated that Macrophages M1 were positively correlated with activated NK cells (r = 0.38), suggesting potential co-participation in pro-inflammatory responses, whereas resting mast cells were negatively correlated with activated mast cells, indicating a relatively suppressed state. Clustering analysis grouped immune cells into functional modules, facilitating understanding of the dynamic regulation of the ovarian cancer immune network. We further analyzed correlations between the expression of previously identified feature genes (SPP1, MAPK13, LCN2, JUP, DSP, BMP6) and immune cell infiltration levels (Figure 7B). Key findings include: SPP1 showed significant positive correlations with memory B cells, Macrophages M0/M2, activated mast cells, and neutrophils (***p < 0.001, *p < 0.05), and negative correlations with naive B cells, resting mast cells, and CD8+ T cells (**p < 0.01, *p < 0.05). MAPK13 was positively correlated with Macrophages M0 and negatively correlated with Tregs and resting mast cells (**p < 0.01, *p < 0.05). LCN2 was positively associated with neutrophils and Tregs (*p < 0.05) and negatively with CD8+ T cells (*p < 0.05). JUP showed positive correlations with memory B cells, Macrophages M0, and Tregs (*p < 0.05). DSP correlated positively with memory B cells and Macrophages M0 (*p < 0.05). BMP6 was strongly positively correlated with resting dendritic cells (***p < 0.001) and negatively with follicular helper T cells (*p < 0.05). Overall, Macrophages M0 emerged as the immune cell type most significantly associated with multiple feature genes (SPP1, MAPK13, JUP, DSP), while SPP1 showed the strongest positive correlation with neutrophils and BMP6 with resting dendritic cells (***p < 0.001). Notably, SPP1 demonstrated significant associations across the widest range of immune cell populations. These gene immune correlations provide insights into potential interactions between specific signaling pathways and the tumor immune microenvironment in ovarian cancer.

Discussion

In this study, we systematically investigated the molecular characteristics of RSRGs in OC and their relationship with the tumor immune microenvironment using integrated multi-dataset analysis and multi-machine learning approaches. Through rigorous preprocessing, batch correction, and differential expression analysis across four GEO datasets, we identified 45 DE-RSRGs. Functional enrichment revealed their involvement in cytoskeletal organization, proteoglycan signaling, lipid metabolism, and the IL-17 pathway biological processes that are closely linked to both tumor progression and stress signaling. Subsequent application of three complementary machine learning algorithms (LASSO, SVM-RFE, and Random Forest) robustly identified six feature genes (SPP1, MAPK13, LCN2, JUP, DSP, and BMP6) as the most critical ribosomal stress–related biomarkers in OC.

Ribosomal stress represents a key node connecting nucleolar function to oncogenic transformation. Disruption of ribosome biogenesis activates signaling cascades that engage p53 and other tumor suppressors to maintain genomic stability. Recent studies have demonstrated that ribosomal stress influences cell proliferation, DNA repair, and metabolic homeostasis in multiple cancers. Our data suggest that ribosomal stress related pathways are aberrantly regulated in OC, with DE-RSRGs enriched in cytoskeletal and integrin-binding functions, which are essential for cell adhesion, invasion, and metastasis. The enrichment of IL-17 and lipid metabolism pathways also implies potential crosstalk between inflammatory signaling and metabolic reprogramming, consistent with evidence that IL-17 promotes pro-inflammatory microenvironments and enhances tumor growth in OC. Moreover, recent studies have demonstrated that inhibition of the IL-17A/IL-6 axis and the MEK1/2 and ERK1/2 signaling pathway can alleviate symptoms in rat models of premature ovarian insufficiency, further supporting the critical role of IL-17 mediated signaling in ovarian pathology. These results highlight ribosomal stress not merely as a bystander response but as an active participant in the molecular pathogenesis of OC.

Among the six feature genes identified through multi-machine learning integration, SPP1 (secreted phosphoprotein 1, also known as osteopontin) emerged as the top-ranked gene by SHAP importance. SPP1 is a multifunctional glycoprotein implicated in extracellular matrix remodeling, immune regulation, and chemoresistanceis a multifunction al matricellular phosphoglycoprotein that is overexpressed in ovarian cancer [9,10]. Clinically, OPN is a serum biomarker for ovarian cancer detection.In addition, elevated OPN in blood and ascites fluid is associated with platinum resistance and poor sur vival in ovarian cancer [11]. OPN signals through CD44 and integrin receptors to activate multiple downstream signaling path ways, including PI3K/AKT, MEK/ERK, and JAK/STAT pathways. Functionally, OPN promotes metastasis, proliferation, stem-like phenotypes, chemoresistance, radiation resistance, and immune suppression in a variety of cancer type. However, the regulation and functional role of OPN in ovarian cancer are poorly defined.

The use of multi-machine learning approaches combining LASSO, SVM-RFE, and Random Forest, enabled robust feature selection from a high-dimensional dataset, effectively minimizing algorithm-specific bias. The convergence of results across three independent methods underscores the reliability of the identified six-gene signature .This integration of predictive modeling and biological interpretation represents an important advancement in bioinformatics-based cancer research, bridging computational accuracy with biological plausibility. Several limitations should be acknowledged. First, this study was based on retrospective transcriptomic data from public databases, lacking experimental validation at the protein or cellular level. Second, although multi-machine learning integration improves robustness, the sample size remains relatively limited, and external validation in independent clinical cohorts is necessary. Future studies should investigate the mechanism of SPP1 invitro in vivoinovarian cancer. It will elucidate the therapeutic potential of targeting the ribosomal stress axis.

Conclusion

This study identified six key ribosomal stress related genes in ovarian cancer, including SPP1, MAPK13, LCN2, and BMP6, linking ribosomal stress to OC. Our integrative framework provides a strategy for exploring the ribosomal stress axis in OC.

Acknowledgments

None.

Conflict of Interest

We all declare that we have no conflict of interest.

Funding

None.

Author Contribution

Xuechuan Han conceived and designed research. Xuechuan Han, Yan Yu conducted experiments. Yang Fan analyzed data. Xuechuan Han wrote the manuscript. All authors read and approved the manuscript.

Data Availability

The simulation experiment data used to support the findings of this study are available from the corresponding author upon request.

Ethical Standards

This study was approved by the Institutional Review Board of People's Hospital of Ningxia Hui Autonomous Region.

References

1. Bray F, Laversanne M, Sung H, Ferlay J, Siegel RL, et al. (2024) Global cancer statistics 2022: GLOBOCAN estimates of incidence and mortality worldwide for 36 cancers in 185 countries. CA Cancer J Clin 74(3): 229-263.
2. Sung H, Ferlay J, Siegel RL, Laversanne M, Soerjomataram I, et al. (2021) Global Cancer Statistics 2020: GLOBOCAN Estimates of Incidence and Mortality Worldwide for 36 Cancers in 185 Countries. CA Cancer J Clin 71(3): 209-249.
3. Dalmartello M, La Vecchia C, Bertuccio P, Boffetta P, Levi F, et al. (2022) European cancer mortality predictions for the year 2022 with focus on ovarian cancer. Ann Oncol 33(3): 330-339.
4. Siegel RL, Kratzer TB, Wagle NS, Sung H, Jemal A (2026) Cancer statistics, 2026. CA Cancer J Clin 76(1): e70043.
5. Konstantinopoulos PA, Matulonis UA (2023) Clinical and translational advances in ovarian cancer therapy. Nat Cancer 4(9): 1239-1257.
6. Giuseppe Caruso, S John Weroha, William Cliby (2025) Ovarian Cancer: A Review. JAMA 334(14): 1278-1291.
7. Kim JY, Cho YE, An YM, Kim SH, Lee YG, et al. (2015) GLTSCR2 is an upstream negative regulator of nucleophosmin in cervical cancer. J Cell Mol Med 19(6): 1245-1252.
8. Mohamed J Saadh, Hanan Hassan Ahmed, Radhwan Abdul Kareem, Anupam Yadav, Subbulakshmi Ganesan, et al. (2025) Advanced machine learning framework for enhancing breast cancer diagnostics through transcriptomic profiling. Discover oncology 16(1): 334.
9. Bo Dong, Chunli Wu, Lan Huang, Yu Qi (2021) Macrophage-Related SPP1 as a Potential Biomarker for Early Lymph Node Metastasis in Lung Adenocarcinoma. Frontiers in cell and developmental biology 9: 739358.
10. Hou L, Jiang M, Li Y, Cheng J, Liu F, et al. (2025) Targeting SPP1+ macrophages via the SPP1-CD44 axis reveals a key mechanism of immune suppression and tumor progression in ovarian cancer. Int Immunopharmacol 160:114906.
11. Gao W, Liu D, Sun H, Shao Z, Shi P, et al. (2022) SPP1 is a prognostic related biomarker and correlated with tumor-infiltrating immune cells in ovarian cancer. BMC Cancer 22(1): 1367.